Pulse Wave Analysis by Quantified Reconstructed Attractors

Carina Hörandtner[1,2], Martin Bachler[1], Siegfried Wassertheurer[1], Felix Breitenecker[2], Christopher C. Mayer[1*]

[1]Biomedical Systems, Center for Health & Bioresources, AIT Austrian Institute of Technology, Giefinggasse 4, 1210 Vienna, Austria; *christopher.mayer@ait.ac.at*

[2]Institute of Analysis and Scientific Computing, Vienna University of Technology, Wiedner Hauptstraße 8–10, 1040 Vienna, Austria

SNE 32(2), 2022, 69-78, DOI: 10.11128/sne.32.tn.10603
Received: 2021-07-21, Revised: 2021-10-10;
Accepted: 2021-12-15
SNE - Simulation Notes Europe, ARGESIM Publisher Vienna,
ISSN Print 2305-9974, Online 2306-0271, www.sne-journal.org

Abstract. Direct time domain analysis is a classical method for pulse wave analysis. Attractor reconstruction is a new and alternative way to analyse the morphology of a pulse wave. The novel approach plots the pulse wave data as overlapping loops in the three-dimensional phase space and, subsequently, projects the trajectories onto a plane generating two-dimensional attractors. This paper presents methods that automatically quantify these attractors. At first, a short overview of the attractor reconstruction technique is provided. After preprocessing of the pulse waveform data, the attractor is generated and edited by a median filter to remove remaining artefacts that can distort the quantification process. The developed algorithm is based on image processing and extracts attractor features such as the angle of rotation, the angle between the arm fragments, shape, height, lengths and width of the attractor. Finally, visual examination evaluates the performance of the feature extraction technique revealing that the majority of the generated attractors are correctly quantified. However, it also shows that remaining outliers and metrological discrepancies have a negative impact on the results.

Introduction

Pulse waveform analysis (PWA) plays an import role in detection and prevention of cardiovascular diseases [1, 2, 3]. Although many approaches of current pulse waveform analysis have proven to be useful tools in early risk assessment, some downsides are worth mentioning. The first issue of PWA is that not all available data is used [4]. Proper inspection and interpretation of a large quantity of data points is an almost impossible or costly task; thus, only average values such as the average interval length or the average maximum and minimum peak values (systolic and diastolic pressure) are examined, which, however, might ignore useful information on the pulse wave's shape. Furthermore, it is difficult to detect any changes in shape and variability of the pulse waveform when it is plotted against a time axis and viewed over a long period of time [4]. Consequently, the pulse waveform can only be quantified appropriately if a short time window is selected which again just focuses on a small number of sampled data. Another issue is baseline wander and noise which can interfere with the signal and may prevent proper quantification [4]. Therfore, baseline wander is removed in some studies [5]. However, editing the original signal might exclude important information from the data.

To overcome these issues, Nandi et al. [4] and Aston et al. [6] developed a new way to visualize and quantify cardiovascular waveform data. The introduced attractor reconstruction method uses every single data point of the sampled waveform, neglects baseline wander and represents pulse waveform signals in a compact three-dimensional phase space which may provide deeper understanding of physiological changes within the cardiovascular system.

In this paper, the method of reconstructing attractors from pulse waveform data is used and further developed [4, 6]. The goal is to present a newly implemented algorithm for the automatic quantification of these attractors.

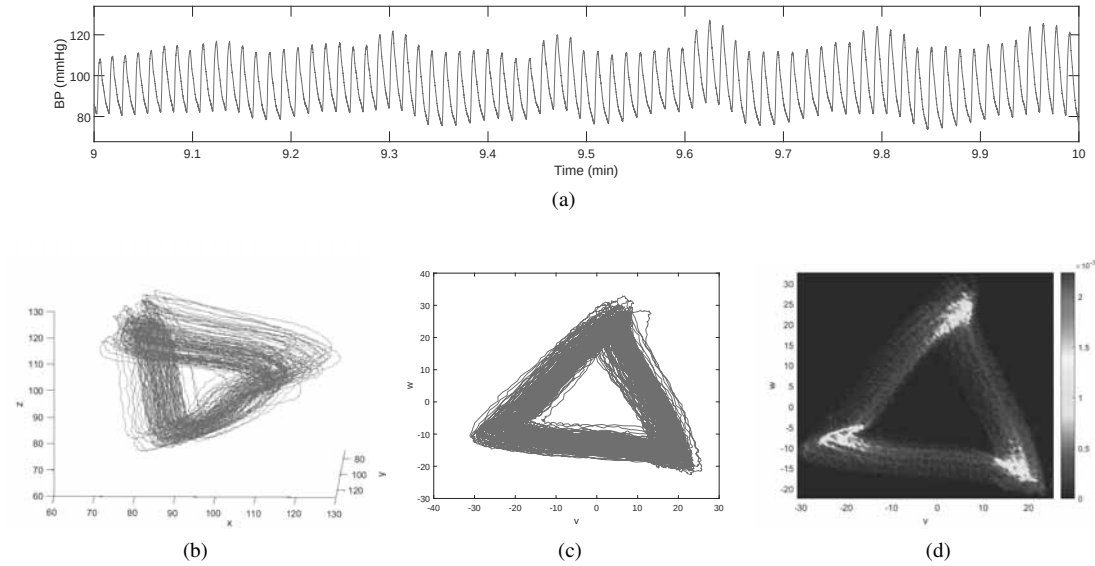

Figure 1: Attractor reconstruction using delay coordinates. (a) 60 second sample of pulse waveform data, (b) reconstructed attractor in the three dimensional phase space, (c) projection of the attractor onto a plane orthogonal to the vector $(1,1,1)$, (d) density plot of the two dimensional attractor.

1 Attractor Reconstruction

The attractor reconstruction method [4, 6] uses Takens' delay coordinates [7] to reconstruct all data points of a cardiovascular waveform (see figure 1a) as a compact object in the three-dimensional phase space. The time delay $\tau > 0$ is chosen to be one third of the average cycle length [6]. Let $x(t)$ be the given signal. Then the two other coordinates are calculated as

$$y(t) = x(t-\tau), \qquad z(t) = x(t-2\tau). \tag{1}$$

The data can then be plotted in the three-dimensional phase space as $(x(t), y(t), z(t))$ for all t in a given time window, resulting in numerous overlapping loops, the so-called attractor (see figure 1b). In order to remove the effect of baseline wander, the three-dimensional attractor is projected onto a plane orthogonal to the vector $(1,1,1)$. The resulting new set of coordinates (u,v,w) is defined as

$$u = \frac{1}{3}(x+y+z), \quad v = \frac{1}{\sqrt{6}}(x+y-2z), \quad z = \frac{1}{\sqrt{2}}(x-y). \tag{2}$$

The two-dimensional attractor in the (v,w) plane (see figure 1c) consists of many overlapping lines with little detail visible. To provide more information on the attractor and to enable the quantification and extraction of attractor features, a density is constructed (see figure 1d).

2 Methodology and Implementation

In order to detect changes in shape and variability of a cardiovascular waveform, the attractors have to be quantified in an automatic manner. In this paper, a method based on pulse waveform data acquired through photoplethysmography at the fingertip is presented. The data sets originate from a pilot study [8] that investigates the impact of device-guided breathing on thirty patients with treated hypertension. Each data set is fifteen minutes long. To generate a sound attractor which provides as much information as necessary, signal segments of 100 seconds are chosen [4]. All parameters and thresholds used in the described algorithms are empirically chosen for the data set at hand, if not stated otherwise. All implementations are done in MATLAB 2019b (The MathWorks, Inc, Natick, MA).

2.1 Preprocessing and Filtering

Preprocessing. Since the attractor reconstruction method uses every single data point, hardly any data

preprocessing is needed, which makes it more resistant to bias introduction [4]. Nevertheless, non-physiological artefacts should be removed because outliers can possibly distort the extraction of attractor features. In this paper, non-physiological outliers are detected in sections with a length of four seconds. To detect possible artefacts, the minima and maxima and their differences are determined and the built-in MATLAB function *isoutlier* is used to discover outliers in the set of the maximum-to-minimum differences. An outlier is characterized by an element that is more than three scaled Median Absolute Deviation (MAD) defined as

$$\mathrm{MAD} = -\frac{1}{\sqrt{2}\cdot \mathrm{erfcinv}(\frac{3}{2})}\cdot \mathrm{median}(|x-\mathrm{median}(x)|), \tag{3}$$

from the median [9]. Here x denotes the vector of the maximum-to-minimum differences and *erfcinv* is the inverse complementary error function. Afterwards, all segments containing artefacts are removed.

Attractor Reconstruction. After removing outliers from the signal, the attractor is generated according to the steps explained in section 1. The density is constructed by using a square grid of 100×100 boxes and the volume is normalized to be one, generating a 100×100 density matrix N.

Median Filter. In order to remove remaining noise which might distort later calculations, a two-dimensional median filter is applied to the density plot of the attractor [10]. For each pixel in the 100×100 density plot a 3×3 neighbourhood is chosen which proves to be suitable for the data used in this paper. The pixel located in the center of the neighbourhood is set to the median value of the pixels within the kernel frame

$$N'(x,y) = \mathrm{median}(N(x+i,y+j),(i,j) \in \{-1,0,1\}). \tag{4}$$

Entries that are smaller than half the size of the median filter kernel value are removed by the filter [10]. In order to eliminate artefacts (see figure 2a) but still preserve the basic structure of the attractor, all values of N, which have not been removed by the median filter, stay the same and the others are set to zero:

$$N(x,y) = \begin{cases} 0, & if\ N'(x,y) = 0, \\ N(x,y), & if\ N'(x,y) \neq 0. \end{cases} \tag{5}$$

Figure 2b shows an attractor after applying the two-dimensional median filter.

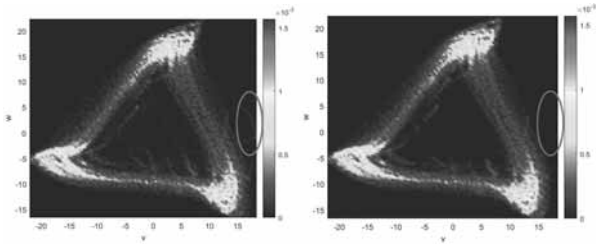

(a) (b)

Figure 2: Application of a two-dimensional median filter with a 3×3 neighbourhood. (a) Unfiltered attractor with artefacts characterized by chaotic lines in the middle and on the right side (exemplarily circled in red), (b) filtered attractor.

2.2 Rotation of the Attractor

After reconstruction and filtering, the attractor has to be rotated. This provides information on the downstroke of the attractor [4, 6] and simplifies further calculations. Figure 3a depicts an attractor in its original form with blurred edges which makes feasible computation more difficult. To overcome this issue and properly detect edges and eventually straight lines, the density matrix N is converted into a binary image using techniques from image processing. In the following, the used MATLAB functions are provided:

```
N = double(N>=(m*max(N(:))));
BW = edge(N,'Prewitt','horizontal');
[H,T,R] = hough(BW);
P  = houghpeaks(H,2,'threshold',...
ceil(0.3*max(H(:))));
lines = houghlines(BW,T,R,P,...
'FillGap',15,'MinLength',len);
```

In order to neglect remaining outliers, all entries of the density matrix N that are greater than $m = 1\%$ of its maximum entry are set to 1 and all others are set to 0. The built-in MATLAB function *edge* finds edges in the binary image that are approximately horizontal (see figure 3b). To detect lines and their position and angle in the image, Hough transform [11] is

used. The function *hough* is designed to detect lines in a binary image BW, where the parameter representation $\rho = x\cos(\theta) + y\sin(\theta)$ of a line is used. Here ρ denotes the perpendicular distance from the origin to the line and θ the angle between the x-axis and this perpendicular vector. The function also returns the parameter space matrix H, whose rows and columns correspond to ρ and θ values, respectively [12]. Any point within the image is mapped to a sinusoidal curve in the Hough space and if two points are located on the same line segment, the two generated curves in the Hough space overlap [13]. The function *houghpeaks* locates peaks, i.e. overlapping sinusoidal curves, in the Hough transform matrix H and returns the column coordinates of the peaks. In this paper, a maximum of two line segments in the image space are considered and the minimum value recognized as a peak is 30% of the maximum value of H. The function *houghlines* extracts the line segments in the image BW (see figure 3c) and returns their angle and position, whereas only lines with a minimum length of $len = 30$ pixels and an angle of 15 degrees above or below the horizontal line are considered. This ensures that only the lower and thus longer edge of the attractor arm is approximated. If no line matches these conditions, the angle of rotation θ is set to NaN, otherwise θ is defined as the mean value of the feasible angles. Afterwards the attractor is rotated in an anticlockwise direction by $\theta \neq NaN$ in the (v,w) plane (see figure 3d):

$$\begin{bmatrix} v_{rot} \\ w_{rot} \end{bmatrix} = \mathrm{R} \cdot \begin{bmatrix} v \\ w \end{bmatrix}, \qquad \mathrm{R} = \begin{bmatrix} \cos(\theta) & -\sin(\theta) \\ \sin(\theta) & \cos(\theta) \end{bmatrix} \tag{6}$$

2.3 Angle between Attractor Arms

Depending on the used signal, attractors can vary in shape. In this study, some attractors have noticeable bent sides, so the next features to be calculated are the angles between the attractor arms β (see figure 4). Because only the shape of the attractor and not the density of different regions is of relevance, the density matrix N is converted into a binary matrix using only values that are greater than 5% of its maximum value; others are set to 0. Investigations of the generated attractors have shown that the bend of the arm is usually located in the south east quarter of the attractor. Therefore, a search window is set to this area of the density matrix. The angle β is defined as $\beta = 180° - \alpha$, thus, the angle α has to be determined first. For this purpose, the attractor is gradually rotated in an anticlockwise direction (see formular 6). In this study, an angle between 0 and 60 degrees and a step size of about $\frac{\pi}{300}$ degrees are used. After each step of the rotation the row sum within the search window and the difference between adjacent values of this row sum vector are calculated. The more horizontal the right fragment of the lower attractor arm gets, the higher is the negative difference in the row sum vector. In each step the minimum value of the vector is determined and stored. After the rotation is completed, i.e. 60 degrees are reached, the minimum value in the vector of minima and its index $i^\star$ are calculated. This yields the sought angle $\alpha^\star = \alpha(i^\star)$ and, consequently, $\beta = 180° - \alpha^\star$. Due to the choice of the time delay τ, the attractor has arbitrary 3-fold rotational symmetry [6]. Thus, the angles between the arm fragments of the two remaining sides are calculated similarly after rotating the attractor by 120 and 240 degrees, respectively, to improve accuracy.

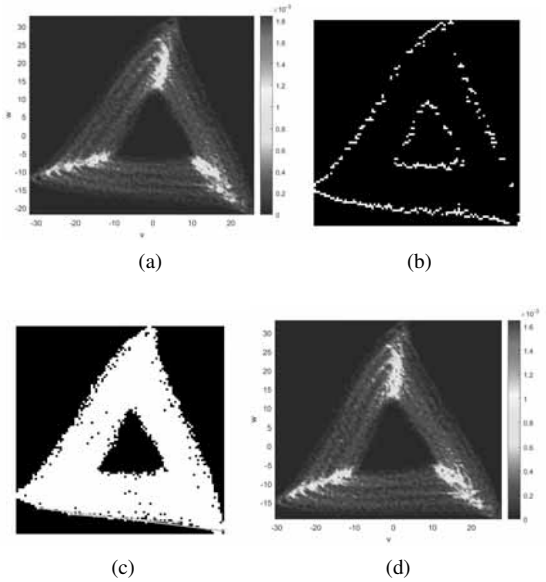

Figure 3: Rotation of the attractor. (a) Original attractor, (b) edge detection in binary image, (c) line detection via Hough transform, (d) rotated attractor.

The developed algorithm automatically categorizes the attractors in two different shapes: triangular attractors (see figure 5a) and attractors with bent sides (see figure 5b). An attractor is said to be triangular in shape, if at least two of the three angles between the attractor arms are greater than or equal to 165 degrees. Other-

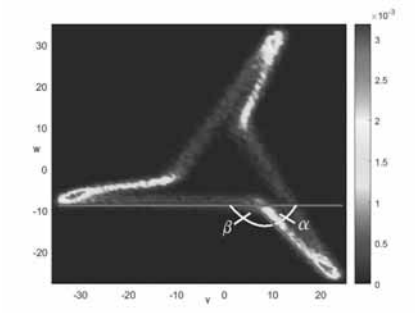

Figure 4: Angle between attractor arm fragments.

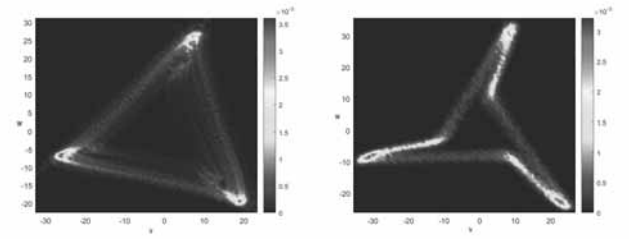

(a) (b)

Figure 5: Different shapes. (a) Triangular attractor, (b) attractor with bent sides.

wise, its shape is understood as bent. This classification is necessary to prevent falsely calculated measurements in the further feature extraction process.

2.4 Lengths and Heights of the Attractor

As opposed to triangular attractors, bent attractor arms consist of two parts, whereas the more horizontal edge is referred to as length a and the other one as length b (see figure 6a). In order to determine these lengths and the heights of the attractors, first the column sum of the density matrix N is calculated. To neglect remaining outliers, only entries greater than or equal to 5% of the column sum vector are considered. The first feasible entry denotes the v-coordinate of the leftmost point and the last entry denotes the v-coordinate of the rightmost point of the attractor. Then, the row sum of the density matrix N is calculated and again only entries greater than or equal to 5% of the vector's maximum value are considered as feasible. The position of the first entry denotes the w-coordinate of the highest point of the attractor. Since the lowest point of the attractor is usually located in the south east quarter of the density plot, only columns right of center are considered. The position of the last entry of the row sum vector of the adjusted matrix labels the w-coordinate of the lowest point. In order to detect the position of the approximately horizontal edge of the attractor, the density plot is converted into a binary image and Hough transform is applied. To find a feasible representative, only lines of 12 degrees above or below the horizontal line are considered as suitable. If two lines fulfil this condition, the lower one is chosen. The horizontal line through the w-coordinate of the middle point of the extracted line represents the lower edge of the attractor. Then, the height h of the attractor is defined as

$$h = \begin{cases} h\_p_w - l\_p_w, & \text{if } l\_p_w < h\_line, \\ h\_p_w - h\_line, & \text{otherwise,} \end{cases} \tag{7}$$

where h_p_w and l_p_w label the w-coordinates of the highest and lowest point, respectively, and h_line denotes the vertical position of the horizontal line. If the considered attractor is triangular in shape, the length of the lower edge a is calculated as

$$a = rm\_p_v - lm\_p_v, \tag{8}$$

where rm_p_v and lm_p_v denote the rightmost and leftmost point, respectively. In case of triangular attractors, the length b is set to zero (see figure 6b). If the attractor has bent arms, the length b is determined by

$$b = \frac{|l\_p_w - h\_line|}{\sin(\alpha)}. \tag{9}$$

The maximum value in the row of the density matrix corresponding to the w-coordinate of the lowest point denotes its v-coordinate. The edge of the attractor with length b is approximated by a straight line with the following parameters:

$$k = \tan(-\alpha), \qquad d = l\_p_w - l\_p_v \cdot k. \tag{10}$$

The length a of the bent attractor is calculated by the difference between the leftmost point and the intersection between the horizontal line and the straight line representing the edge with length b (see figure 6a).

To compare different attractors, the ratio $\frac{b}{a}$ is built. Due to 3-fold rotational symmetry, the process can be repeated after rotating the attractor by 120 and 240 degrees to improve accuracy.

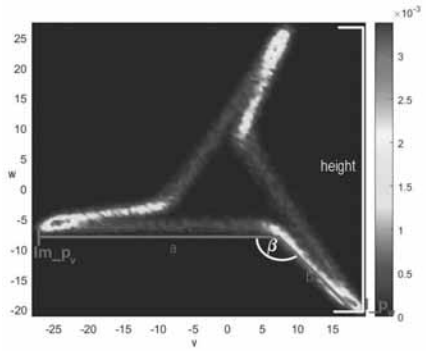

(a)

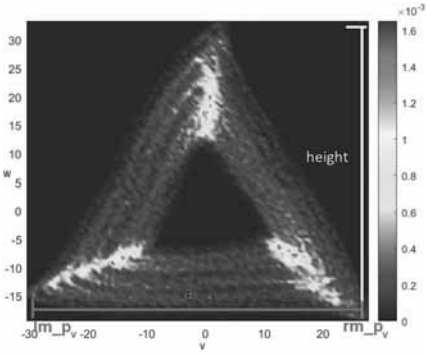

(b)

Figure 6: Lengths and heights of the attractor. (a) Measurements of a bent attractor, (b) measurements of a triangular attractor.

2.5 Width of the Attractor

The width of the attractor arm measures the variability of a waveform [4, 6]. In order to properly determine the width of one side, a search window is placed on the density plot (see figure 7). In case of triangular attractors, which are approximately symmetrical about the *w*-axis, the search area is located in the middle of the lower arm. Bent attractors tend to have a smaller gap between the attractor arms, especially on the left side. Thus, 75% of the search window is placed right of the center which has proven to be suitable for the given data set. The other two arms should not affect the calculations; therefore, the size of the window is chosen as slim as possible to cover a significant area but to guarantee no distortion because of the two other sides. In this paper, 10% of length a has granted the best results for the given data set. The width of the attractor arm is determined by a combination of two methods. The first method detects large density differences in the density plot and the second method uses triangular interpolation similar to the Triangular Interpolation of the NN Interval Histogram (TINN) [14].

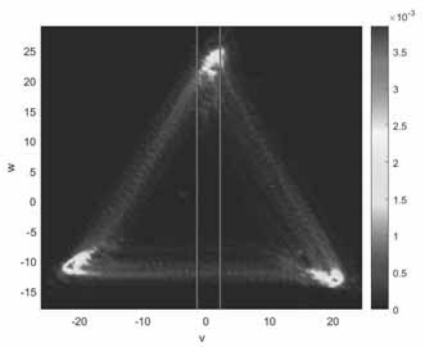

Figure 7: Triangular attractor with placed search window to determine the width of the attractor arm.

1st Method. The first method focuses on the largest density differences within the search window and returns the upper and lower limit of the attractor band. For that purpose, the row sum vector of the density matrix within the search area is calculated. In order to to find the beginning and the ending of the attractor arm, all entries, which are greater than or equal to 1% of the vector's maximum value, and their positions are determined. The index differences of the determined entries highlight possible density gaps within the window, i.e. jumps from high to very low density regions near zero and jumps back to high density regions. In this study, a gap of at least 3 indices is considered as sufficient for the given data set. The position of the upper limit of the attractor band is marked by the end of the gap, whereas the position of the lower limit is presented by the position of the last entry of the row sum vector.

2nd Method. The second method uses the ideas introduced in [14] and determines the upper and lower limit of the attractor arm by fitting a triangle to the density function in a least square sense. The triangular interpolation is depicted in figure 8, where A denotes the lower limit and B the upper limit of the arm. $D(i)$ represents the values of the row sum vector of the density matrix limited to the search window. In order to guarantee that only the lower attractor band is considered, the method only focuses on the lower 40% of the attractor, which has proven to be suitable for the given data set. To calculate the edges of the triangle, a piecewise linear function $t(w)$ is used:

$$t(w) = \begin{cases} 0, & w \leq A, \\ t_1, & A \leq w \leq D_{max}, \\ t_2, & D_{max} \leq w \leq B, \\ 0, & B \leq w \leq L. \end{cases} \tag{11}$$

D_{max} denotes the position of the highest density value and L marks the limit of the lower 40% of the attractor. In order to determine the limits A and B, the integral over the squared difference $(D(w) - t(w))^2$ has to be minimized, i.e.

$$\int_{-\infty}^{L} (D(w) - t(w))^2 dw \to 0. \tag{12}$$

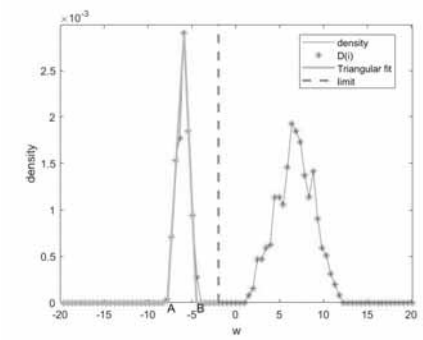

Figure 8: Triangular interpolation of the density function to get the upper limit B and the lower limit A. The width of the attractor arm is defined as $B - A$.

The performance of both methods varies in success depending on the given data set. Therefore, a combination of the two methods is applied to guarantee a proper calculation of the width of the attractor arm (see figure 9). Usually the highest upper boundary and the lowest lower boundary are used with a few exceptions, which have proven to be necessary for the given data set:

- If the upper limit of the first method is higher than $B + 1.5 \cdot (B - A)$, the upper limit is set to B. This constraint ensures that remaining outliers located in the middle of the attractor do not distort the upper boundary.
- Sometimes the second method determines boundaries too generously. If B is higher than the upper limit of the first method but there are no attractor lines between those two values within the search window, the upper boundary of the first method is used.

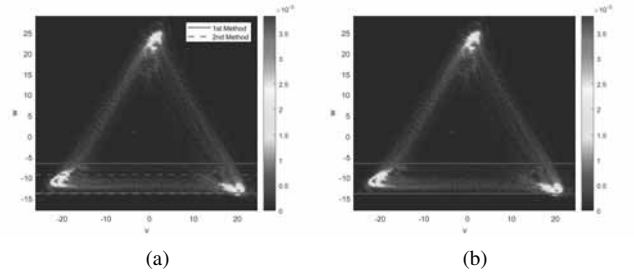

Figure 9: Width of the attractor arm. (a) Upper and lower limits calculated by both methods, (b) combination of the two methods.

- If the lower limit is lower than $A - 0.8 \cdot (B - A)$, the lower boundary is set to A. Again, this ensures that possible outliers have no negative impact on the lower limit.
- If A is lower than the lower limit of the first method but there are no attractor lines between those two values within the search window, the lower boundary of the first method is used to guarantee that the attractor arm is as narrow as possible.

After determining the upper and lower boundary, the width of the attractor arm is defined as the difference between the upper and lower limit. Due to the 3-fold rotational symmetry of the attractor, the procedure can be repeated after rotating the attractor by 120 and 240 degrees to improve accuracy.

3 Results

In order to evaluate the feature extraction method, 90 (three per subject) pulse wave signals chosen at the beginning, after 10 minutes and at the ending of the recording and the corresponding attractors are visually examined. Most of the generated triangular and bent attractors are correctly rotated, as illustrated in figure 10a–10b and figure 11a–11b. The quality of the given data set is crucial for proper quantification of the attractors as remaining outliers lead to chaotic behaviour of the attractors and, as a consequence, to a miscalculation of the angle of rotation θ. Remaining artefacts have a negative impact on two of the 90 attractors and their rotation, as depicted in figure 12a–12b. Further calculations, i.e. the determination of the angle between the attractor arm fragments β and the lengths and widths of the arms, are dependent on the correct rotation. 14 (16%) attractors are triangular in shape and lengths and

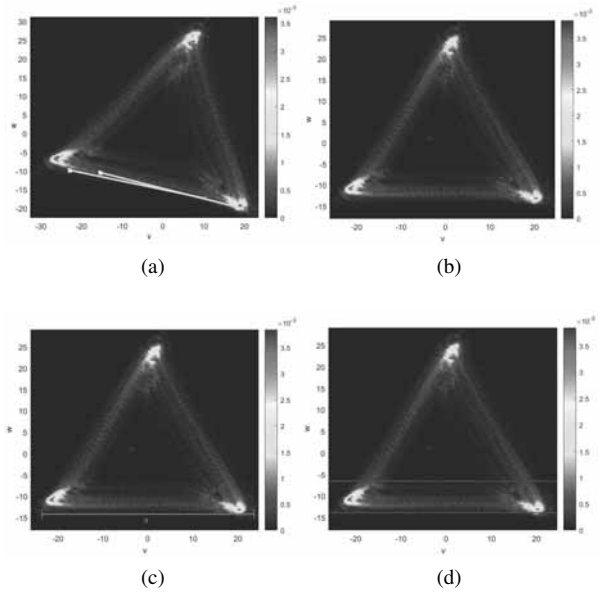

Figure 10: Triangular attractor with correctly extracted features. (a) Attractor with properly detected lower edge, (b) rotated attractor, (c) length of the attractor arm, (d) width of the attractor arm.

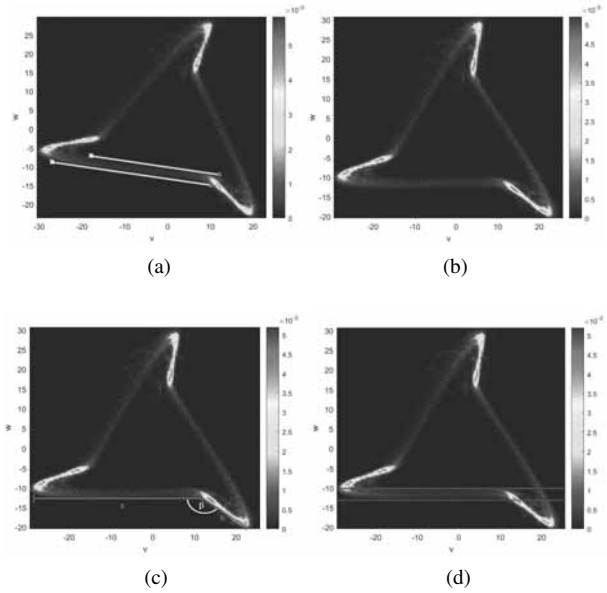

Figure 11: Bent attractor with correctly extracted features. (a) Attractor with properly detected lower edge, (b) rotated attractor, (c) lengths of the attractor arm, (d) width of the attractor arm.

widths of the attractor arms are determined accurately (see figure 10c–10d). The magnitude of the bent attractors are correctly quantified as well, as depicted in figure 11c–11d. However, due to outliers and miscalculations of the angle of rotation θ, the quantification of four attractors is inaccurate. Figure 12c and figure 12d illustrate the wrongly calculated angle between the attractor arm fragments β and, consequently, the incorrectly determined lengths and widths of the attractor arms.

Visual examination also shows that three (3%) attractors are divided into two parts: a smaller attractor with a high density and a larger attractor consisting of only a few lines (see figure 13a). This partitioning is thought to be caused by metrological effects, like varying pressure on the recording device, which lead to a rapid increase in the signal's amplitude and cannot be detected by the preprocessing method or median filtering. Although the two attractor parts seem to have some similar features, like the angle or rotation and the angle between the arm fragments, the attractor cannot be quantified satisfactorily. The lengths and heights of the attractor refer to the larger attractor part (see figure 13c), whereas the arms widths are extracted from the smaller part with a higher density (see figure 13d).

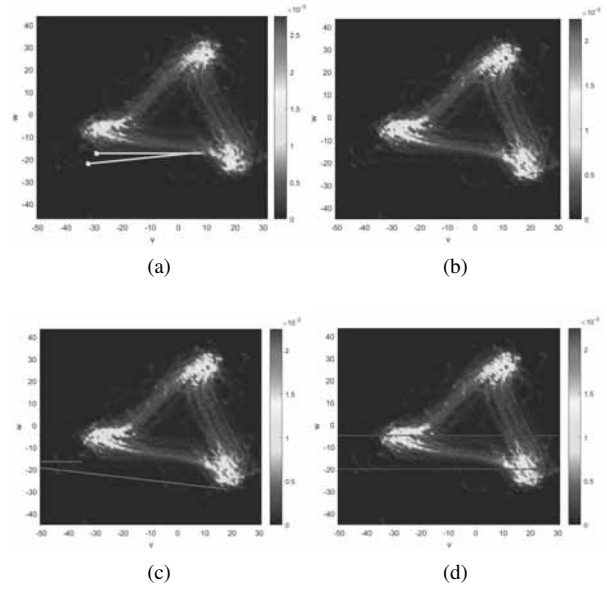

Figure 12: Incorrectly quantified attractor. (a) Attractors with a lot of outliers, (b) incorrectly rotated attractor, (c) incorrect extraction of the attractor arm length represented in red, (d) incorrect determination of the attractor arm width.

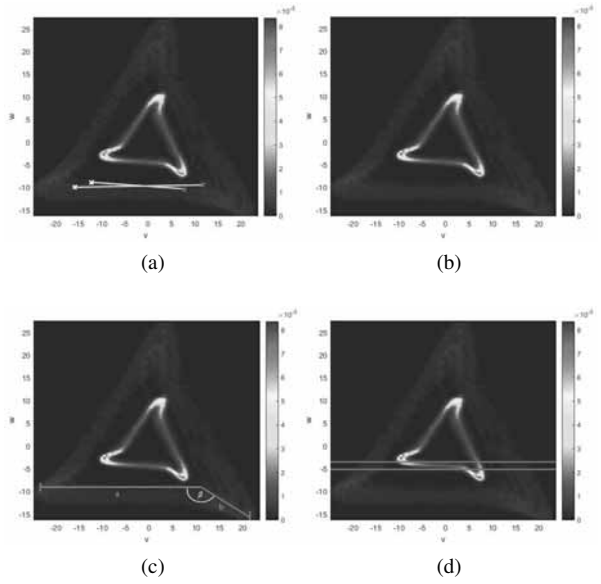

Figure 13: Incorrectly quantified attractor. (a) Attractor consisting of a small attractor with high density and a large attractor with low density, (b) incorrectly rotated attractor, (c) determination of the attractor arm lengths. The applied algorithm focuses on the larger part of the attractor. (d) Calculation of the arm width with a focus on the smaller part of the attractor with high density.

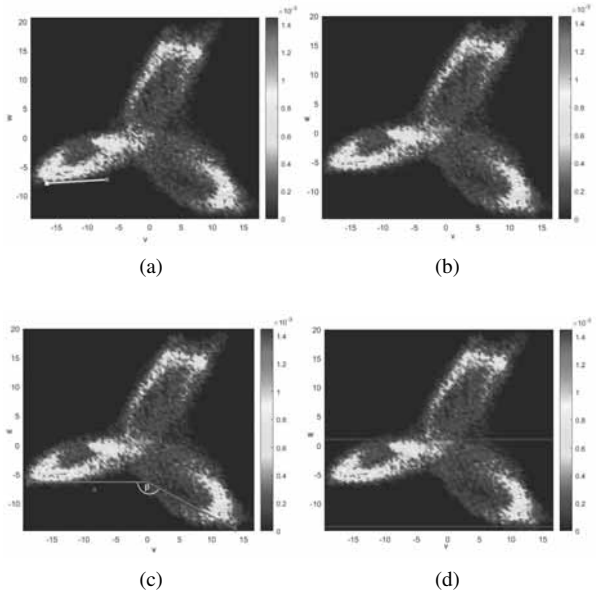

Figure 14: Incorrectly quantified attractor due to its shape. (a) Attractor with overlapping arms, (b) incorrectly rotated attractor, (c) inaccurate extraction of the angle between the attractor arms and the lengths of the attractor, (d) incorrect determination of the attractor arm width.

The developed method classifies the attractors into two different shapes: triangular and bent attractors. However, visual examination reveals that three attractors differ in shape and have overlapping arms (see figure 14a). Because of the distinct loops, the attractors cannot be assigned accurately to one of the predefined shapes which complicates further calculations. The overlapping arms distort the angle of rotation (see figure 14a–14b) and determine an incorrect angle between the attractor arm fragments (see figure 14c). Furthermore, the widths of the attractor arms cannot be calculated satisfactorily. Due to the loops, there is no gap in the middle of the attractor, which is an essential condition for determination of the arm width as explained in section 2.5. The missing gap leads to a much broader arm width, as seen in figure 14d.

4 Conclusion and Outlook

In this paper, an algorithm for the automatic quantification of attractors reconstructed from pulse waveform data is presented. The feature extraction technique mainly focuses on a combination of image processing together with the usage of the 100×100 density matrix. Visual examination of the quantified attractors reveals high accuracy of the algorithm in most cases. However, remaining outliers or metrological effects, such as varying pressure on the recording device, have a negative impact on the correct quantification of the attractors. Additionally, the developed algorithm can only distinguish between triangular and bent attractors but is not able to correctly detect attractors with overlapping sides.

Thus, further improvements of the feature extraction technique that ensure a more stable outcome and classify more attractor shapes would be of advantage. Furthermore, the method has been developed to analyse pulse wave data acquired through photoplethysmography at the fingertip. However, it it is not assured that the algorithm works equally precise on pulse wave signals recorded with an occlusive cuff, electrocardiogram (ECG) signals [15, 16] or other almost periodic signals. Thus, it would be interesting to apply the developed method on these signals as well and, if necessary, adapt the feature extraction technique accordingly.

Acknowledgement

Part of this research was funded by the State of Lower Austria with co-financing from the European Regional Development Fund (ERDF / EFRE) – Project "smart-PWA" / WST3-F-5030665/002-2017.

References

[1] Hametner B. and Wassertheurer S. Pulse Waveform Analysis: Is It Ready for Prime Time? *Curr Hypertens Rep.* 2017 Aug 11;19(9):73. doi: 10.1007/s11906-017-0769-3. PMID: 28801878.

[2] O'Rourke MF., Pauca A., Jiang XJ. Pulse wave analysis. *British journal of clinical pharmacology*. 2001; 51(6):507-522. doi: 10.1046/j.0306-5251.2001.01400.x.

[3] Wilkinson IB., Cockcroft JR., Webb DJ. Pulse wave analysis and arterial stiffness. *J Cardiovasc Pharmacol*. 1998; 32 Suppl 3:S33-7. PMID: 9883745.

[4] Nandi M., Venton J. and Aston P. A novel method to quantify arterial pulse waveform morphology: attractor reconstruction for physiologists and clinicians. *Physiol. Meas*. 2018; 39(10):104008. doi: 10.1088/1361-6579/aae46a.

[5] Fedotov AA. and Akulova AS. Adaptive filter for eliminating baseline wander of pulse wave signals. *World Congress on Medical Physics and Biomedical Engineering*. June 7-12, 2015, Toronto, Canada. pp 1018-1021.

[6] Aston P., Christie M., Huang Y. and Nandi M. Beyond HRV: attractor reconstruction using the entire cardiovascular waveform data for novel feature extraction. *Physiol.Meas*. 2018; 39(2):024001. doi: 10.1088/1361-6579/aaa93d.

[7] Takens F. Detecting strange attractors in turbulence. In: Rand D., Young LS. editors. *Dynamical Systems and Turbulence*. Springer Berlin Heidelberg. 1981. pp 366-381.

[8] Bachler M., Sehnert W., Mikisek I., Wassertheurer S., and Mengden T. Non-invasive quantification of the effect of device-guided slow breathing with direct feedback to the patient to reduce blood pressure. *Physiol Meas.* 2020; 41(10):104002. doi: 10.1088/1361-6579/abb320.

[9] MathWorksl 2021. MATLAB Function Reference (2021a). Retrieved from `https://de.mathworks.com/help/pdf_doc/matlab/matlab_ref.pdf` [visited on 20/06/2021].

[10] Paranjape R.B. Chapter 1 - fundamental enhancement techniques. In: ISAAC N. BANKMAN editors. *Handbook of Medical Image Processing and Analysis*. 2nd edition, Academic Press, Burlington. 2009. pp 3-18.

[11] Duda R. and Hart P. Use of the hough transformation to detect lines and curves in pictures. *Commun. ACM*. Jan. 1972; 15(1):11-15. doi: 10.1145/361237.361242.

[12] MathWorks, 2020. Image Processing Toolbox User's Guide (R2020a). Retrieved from `https://de.mathworks.com/help/pdf_doc/images/images_ug.pdf`. [visited on 06/15/2020].

[13] Elsalamony H. Chapter 30 - Detecting distorted and benign blood cells using the Hough transform based on neural networks and decision trees. *Emerging Trends in Image Processing, Computer Vision and Pattern Recognition*. Morgan Kaufmann. 2015. pp 457-473.

[14] Task Force of the European Society of Cardiology the North American Society of Pacing Electrophysiology. Heart Rate Variability: Standards of Measurement, Physiological Interpretation, and Clinical Use. *Circulation*. 1996; 93(5):1043-1065. doi: 10.1161/01.CIR.93.5.1043.

[15] Lyle JV. et al. Beyond HRV: Analysis of ECG signals using attractor reconstruction. *Computing in Cardiology (CinC)*. 2017, pp. 1-4, doi: 10.22489/CinC.2017.091-096.

[16] Aston P. et al. Deep Learning Applied to Attractor Images Derived from ECG Signals for Detection of Genetic Mutation. *Computing in Cardiology (CinC)*. 2019, pp. 1-4, doi: 10.23919/CinC49843.2019.9005823.